Infrared and Raman Line Shapes of Dilute HOD in Liquid H_2O and D_2O from 10 to 90 °C

S. A. Corcelli and J. L. Skinner*

Theoretical Chemistry Institute and Department of Chemistry, University of Wisconsin, Madison, Wisconsin 53706

Received: February 6, 2005; In Final Form: May 17, 2005

A combined electronic structure/molecular dynamics approach was used to calculate infrared and isotropic Raman spectra for the OH or OD stretches of dilute HOD in D_2O or H_2O, respectively. The quantities needed to compute the infrared and Raman spectra were obtained from density functional theory calculations performed on clusters, generated from liquid-state configurations, containing an HOD molecule along with 4−9 solvent water molecules. The frequency, transition dipole, and isotropic transition polarizability were each empirically related to the electric field due to the solvent along the OH (or OD) bond, calculated on the H (or D) atom of interest. The frequency and transition dipole moment of the OH (or OD) stretch of the HOD molecule were found to be very sensitive to its instantaneous solvent environment, as opposed to the isotropic transition polarizability, which was found to be relatively insensitive to environment. Infrared and isotropic Raman spectra were computed within a molecular dynamics simulation by using the empirical relationships and semiclassical expressions for the line shapes. The line shapes agree well with experiment over a temperature range from 10 to 90 °C.

I. Introduction

The frequencies of molecular vibrations are extremely sensitive to their local solvation environments. As a result, experimental techniques that probe vibrations, such as infrared spectroscopy and Raman scattering, can be ideal for studying the structure and dynamics of condensed phase systems. For example, in biology infrared spectroscopy has been used to study the elusive structural properties of membrane-bound peptides, either by probing isotopically labeled backbone carbonyl stretches (e.g., $^{13}C^{18}O$)[1,2] or by introducing amino acids whose side chains have been derivatized with CN groups.[3] The vibrational frequencies of the CO or CN probes are sensitive to their degree of hydration (i.e., if they are experiencing a hydrophobic or hydrophilic environment) and to their coupling with other modes.[4−23] To extract as much meaningful molecular-level structural and dynamical information as possible from the experiments, it is important that computational methods be developed that can accurately predict the infrared spectrum of a vibrational probe in a variety of different environments.

The vibrational spectroscopy of liquid water (and also of solutes in aqueous solution) is of paramount interest because of the prominent role of water as a solvent, and sometimes even as an active participant, in biochemical reactions. The OH stretch vibrational spectrum of neat liquid water is complicated by strong intra- and intermolecular coupling of the ensemble of nearly-resonant OH oscillators present in the liquid. To avoid these conceptual difficulties, recent ultrafast studies of the vibrational dynamics of water have focused on the OH stretch of dilute HOD in D_2O,[24−43] or the OD stretch of dilute HOD in H_2O.[44−50] In these isotopic mixtures the OH or OD vibration of interest is spectrally isolated from all of the other modes present in the liquid, and to an excellent approximation can be considered as an uncoupled local mode. This important simplification allows the crucial role of the solvent environment on the spectroscopy and dynamics of the vibration of interest to be studied separately from the effects of vibrational coupling.

The infrared[46,51−55] and isotropic Raman[51,56−59] spectra of dilute HOD in H_2O and D_2O have been widely reported at a variety of liquid-state temperatures. At room temperature the infrared and isotropic Raman spectra are not the same: the isotropic Raman line shape displays a characteristic shoulder on the blue side of the spectrum that is absent in the infrared spectrum, and the entire infrared spectrum is red-shifted relative to the Raman spectrum.[53] The shoulder present in the Raman spectrum has been associated with the subensemble of water molecules with weak or broken hydrogen bonds.[40,41,51,59,60] The temperature dependence of the infrared and isotropic Raman spectra is qualitatively different. Most prominently, the blue shoulder present in the Raman spectrum grows in relative intensity with increasing temperature, and remains completely absent in the infrared line shape. Also, while the peak positions of both the infrared and Raman spectra shift to the blue with increasing temperature, the widths of the peaks show different trends with respect to temperature: for the infrared spectrum the width monotonically increases with temperature, but for the Raman spectrum the width first increases and then decreases as the temperature increases.

Although considerable theoretical effort has been devoted to devising strategies for calculating the vibrational frequencies of a solute molecule (such as HOD) in liquid water,[28,61−80] the OH and OD infrared and isotropic Raman line shapes of dilute HOD in D_2O and H_2O have never been calculated (for a given water model) with sufficient accuracy to explain all of the differences observed in the experimental spectra. A substantial theoretical obstacle to an accurate calculation of at least the infrared line shapes is that the transition dipole moment of the OH or OD stretch depends very sensitively on the molecule's hydrogen-bonding environment.[81−84] Most previous works have neglected this (non-Condon) effect, but there have been some efforts to take it into account. For example, Hermansson et al. calculated the transition dipole moment of the OH vibration for 40 clusters each containing an HOD molecule surrounded

10.1021/jp0506540 CCC: $30.25
Published on Web 06/28/2005

by 4 D_2O solvent molecules.[85] The clusters were taken from a Monte Carlo simulation of the MCY model of liquid water,[86] and MP2 electronic structure calculations of the OH frequency and Hartree−Fock level calculations of the transition dipole were performed in the presence of the point charges of the water molecules not explicitly contained in the cluster. Hermansson et al. observed a linear relationship between the transition dipole squared and the OH frequency. IR spectra were not reported but the vibrational density of states of the 40 clusters were weighted by the frequency-dependent transition dipole. Buck, Buch, and co-workers have further applied the linear relationship between OH frequency and transition dipole moment squared derived from the ab initio calculations of Hermansson et al.[85] in their calculations of the spectra of water clusters containing 7−10 molecules.[71−73] Wojcik et al. calculated infrared spectra (excluding the dynamical effects of frequency fluctuations) for the OH and OD stretching bands of dilute HOD in D_2O and H_2O.[87] Vibrational frequencies were calculated by adiabatically varying the OH (or OD) vibrational coordinate over a suitable range (with the solvent held fixed), and solving the resulting Schrödinger equation. For the infrared spectra the vibrational densities of states were weighted by linear empirical relationships of intensity versus frequency obtained from experiments on water molecules in different solvents.[83] Finally, Morita and Hynes have incorporated transition dipole and transition polarizability information into calculations of the sum-frequency-generation spectrum of the air/water interface.[88,89] Density functional theory (DFT) calculations were performed on $Cl^-\cdot(H_2O)_2$ clusters to assess the perturbation of hydrogen bonding on the transition dipole and polarizabilities of water. For the transition dipole moment a linear relationship with frequency was observed, and the transition polarizabilities were relatively insensitive to the degree of hydrogen bonding.

We have recently developed a flexible computational approach for relating the vibrational frequencies of a solute to its molecular environment that combines ab initio electronic structure (ES) methods with molecular dynamics (MD) simulation.[45−47,90−92] The combined ES/MD approach is similar to the one developed and applied to *N*-methylacetamide in aqueous solution by Cho and co-workers.[67−70] The approach begins by extracting clusters of the solute and its local solvent environment from a short MD simulation of the solute/solvent system. The clusters are of a size that are amenable to ES calculations, and are representative of the types of solvation environments experienced by the solute. The vibrational frequencies of the solute are then calculated for each cluster using DFT, typically with the B3LYP functional and a 6-311++G** basis set. The ab initio frequencies are empirically related to the electric field, calculated using the solvent point charges of the simulation model, on various atomic sites of the solute. For the case of the OH (OD) stretch of dilute HOD in D_2O (H_2O), the OH (OD) frequency is linearly correlated with the electric field due to the solvent on the H (D) atom, and projected along the OH (OD) bond. Once the empirical relationship between frequency and field has been established for a given solute/solvent simulation model, the frequencies of the solute can be evaluated within an MD simulation with no further ES calculations. We note that others have also exploited the connection between electric field and frequency.[28,71−73,93−95]

In the present work we extend the combined ES/MD framework to include the quantities needed to compute infrared and isotropic Raman line shapes—namely, the transition dipole moment, μ', and the transition polarizability, α'. These quantities describe how the dipole moment and isotropic polarizability of the HOD molecule change upon an infinitesimal displacement of the H (or D) atom of interest from its equilibrium position in the direction of the OH (or OD) bond. μ' and α' intrinsically depend on the electronic structure of the HOD molecule, which in turn is different for different solvation environments. The quantities μ' and α' are computed for the OH and OD stretches of representative HOD/water clusters with ES methods. μ' and α' are then empirically related to the electric field due to the solvent along the OH or OD bond of interest. Using empirical relationships derived from ES calculations for the frequency, transition dipole, and transition polarizability, the OH and OD infrared and isotropic Raman line shapes for dilute HOD in D_2O and H_2O are calculated using MD simulations performed at temperatures in the range 10 to 90 °C.

We have previously applied the combined ES/MD approach to the calculation of spectral diffusion of the OH and OD vibrations of dilute HOD in D_2O and H_2O.[45−47,90,91] Spectral diffusion dynamics are typically characterized in terms of the frequency time-correlation function (FTCF), $C(t) = \langle \delta\omega(t)\delta\omega(0)\rangle$, where $\delta\omega(t)$ is the fluctuation of the instantaneous anharmonic 0−1 vibrational frequency from its equilibrium value: $\delta\omega(t) = \omega(t) - \langle\omega\rangle$. The FTCF is an important quantity that can be obtained directly from the ES/MD simulation and is measured by time-resolved infrared experiments. The time scales for the decay of the FTCF describe how quickly the frequency loses memory of its initial value (i.e., how quickly the solvation environment loses memory of its initial configuration). Of particular physical and chemical significance is the long-time decay of the FTCF, which we and others attribute to the dynamics of making and breaking hydrogen bonds in the liquid.[61−64] Tokmakoff and co-workers suggest a more general point of view, that the long-time decay involves "the kinetics of randomizing intermolecular hydrogen bonding structure".[26]

In our previous work[90−92] we calculated the FTCF of the OD vibration of HOD in H_2O for three commonly used water models: TIP4P,[96] SPC/E,[97] and SPC-FQ.[98] The long-time decays of the FTCF for the three models were 0.5, 0.9, and 1.45 ps, respectively. The decay of the FTCF as measured in the most recent vibrational echo experiments is about 1.4 ps for HOD in H_2O,[47] and 1.4 ps for HOD in D_2O.[26] Thus it appears (but see ref 99) that the polarizable SPC-FQ model is superior to the nonpolarizable SPC/E and TIP4P models for describing the dynamics of making and breaking hydrogen bonds in liquid water.[100] All three of these commonly used water models have been explicitly parametrized to reproduce the structure of the liquid (i.e., the radial distribution functions extracted from neutron and X-ray scattering experiments[101,102]). The ability of a water model to reproduce infrared and isotropic Raman spectra would attest further to its overall quality. Because of its success in describing the long-time decay of the FTCF, we have chosen to apply the methods developed in this paper exclusively to the SPC-FQ water model.

The paper is organized as follows: In Section II we develop semiclassical approximations for the infrared and isotropic Raman line shapes that are amenable to calculation within the ES/MD framework. Section III details the combined ES/MD methodology as it applies to dilute HOD in water, and empirical relationships for the OH (and OD) stretch frequencies, transition dipole moments, and isotropic transition polarizabilities needed for calculating the infrared and Raman spectra are presented. In Section IVA we discuss our results for the room-temperature OH and OD infrared and isotropic Raman line shapes and their agreement with experiment. Section IVB examines the temper-

ature dependence of the OH and OD infrared and isotropic Raman spectra. Finally, in Section V we make some concluding remarks.

II. Theory

A. Infrared Line Shape. Infrared spectroscopy of HOD in water provides information about the structure and dynamics of the liquid. In particular, the linear infrared absorption line shape for the fundamental vibrational transition of either the OH or OD stretch is sensitive both to the inhomogeneous distribution of solvation environments present in the liquid and to the time scales of the frequency fluctuation dynamics. For the purposes of computing the infrared spectrum within a classical MD simulation it is appropriate to begin with a semiclassical approximation to the absorption line shape,[66,90,103−107]

$$I(\omega) \sim \int_{-\infty}^{\infty} \mathrm{d}t\, \mathrm{e}^{-i(\omega-\langle\omega\rangle)t}\phi_I(t) \tag{1}$$

where the infrared line shape function is

$$\phi_I(t) = \mathrm{e}^{-|t|/2T_1}\langle\vec{\mu}_{01}(0)\cdot\vec{\mu}_{10}(t)\mathrm{e}^{i\int_0^t \mathrm{d}\tau\delta\omega(\tau)}\rangle \tag{2}$$

In the above expression $\delta\omega(t) = \omega(t) - \langle\omega\rangle$ is the fluctuation of the vibrational frequency of interest from its equilibrium value, T_1 is the population relaxation lifetime of the excited vibration, and $\vec{\mu}_{10}$ is the matrix element of the dipole operator between the first excited vibrational state and the ground state for the relevant mode:

$$\vec{\mu}_{10} = \langle 1|\vec{\mu}|0\rangle \tag{3}$$

The angular brackets in eq 2 indicate a classical equilibrium statistical mechanical average. In our numerical calculations we use the experimentally measured values of T_1: 750 fs for the OH stretch of HOD in D_2O,[38,108,109] and 1.45 ps for the OD stretch of HOD in H_2O.[44]

In what follows we will be describing either the OH or OD vibration as a one-dimensional local mode. To evaluate the matrix element in eq 3, the dipole operator is assumed to depend only on $x = r - r_0$, which is the displacement of the OH or OD bond distance of interest, r, from its equilibrium value, r_0. We then expand $\vec{\mu}$ to first order in x:

$$\vec{\mu} = \vec{\mu}_0 + \left(\frac{\mathrm{d}\vec{\mu}}{\mathrm{d}x}\right)_{x=0} x + ... \approx \vec{\mu}_0 + \vec{\mu}'x \tag{4}$$

$\vec{\mu}$ is separated into a magnitude (μ') and a direction ($\hat{u}$): $\vec{\mu}' = \mu'\hat{u}$. Surprisingly, for the isolated water molecule $\hat{u}$ is not along the bond, but rather is rotated by 25.2°.[84] In ice, however, where significant hydrogen bonding is present, $\hat{u}$ is much closer to the bond vector.[84] We are not aware of any experiments that determine the average direction of $\hat{u}$ for the liquid. Certainly, it will be true that $\hat{u}$ depends on the instantaneous hydrogen-bond configuration. Nonetheless, since on the average hydrogen bonding in water is not so different from that in ice, for simplicity here we take $\hat{u}$ to be the bond vector. The matrix element of the dipole operator can now be expressed as

$$\vec{\mu}_{10} = \mu'\langle 1|x|0\rangle\hat{u} \equiv \mu' x_{10}\hat{u} \tag{5}$$

where x_{10} is the matrix element of the vibrational coordinate between the ground and first excited (anharmonic) vibrational eigenstates. The final expression for the infrared absorption line shape function is obtained by substituting the previous equation for the dipole operator matrix element back into eq 2 to give

$$\phi_I(t) = \mathrm{e}^{-|t|/2T_1}\langle\mu'(0)\mu'(t)x_{10}(0)x_{10}(t)\hat{u}(0)\cdot\hat{u}(t)\mathrm{e}^{i\int_0^t \mathrm{d}\tau\delta\omega(\tau)}\rangle \tag{6}$$

The time dependence of all of the quantities (μ', x_{10}, $\hat{u}$, $\delta\omega$) contained within eq 6 will be obtained from a standard MD simulation using the methods described below in Section III.

B. Isotropic Raman Line Shape. To obtain an equation for the isotropic Raman spectrum that can be calculated within an MD simulation, the starting point is once again a semiclassical expression for the isotropic Raman line shape function,[107,110−112]

$$\phi_R(t) = \mathrm{e}^{-|t|/2T_1}\langle\alpha_{01}(0)\alpha_{10}(t)\mathrm{e}^{i\int_0^t \mathrm{d}\tau\delta\omega(\tau)}\rangle \tag{7}$$

α_{10} is the matrix element of the isotropic polarizability operator between the ground and excited vibrational states:

$$\alpha_{10} = \langle 1|\alpha|0\rangle \tag{8}$$

where

$$\alpha = \frac{1}{3}(\alpha_{xx} + \alpha_{yy} + \alpha_{zz}) \tag{9}$$

The isotropic Raman spectrum is given by the Fourier transform of eq 7 as in eq 1.

To evaluate the matrix element defined by eq 8 the isotropic polarizability operator is expanded to linear order with respect to the vibrational coordinate x:

$$\alpha = \alpha_0 + \left(\frac{\mathrm{d}\alpha}{\mathrm{d}x}\right)_{x=0} x + ... \approx \alpha_0 + \alpha' x \tag{10}$$

where α' is the transition polarizability—the derivative of the molecular polarizability with respect to the vibrational coordinate x. Using this expansion for the isotropic polarizability operator, the matrix element in eq 8 is evaluated to give

$$\alpha_{10} = \alpha'\langle 1|x|0\rangle = \alpha' x_{10} \tag{11}$$

The final equation for the isotropic Raman line shape function can be arrived at by substituting this equation back into eq 7:

$$\phi_R(t) = \mathrm{e}^{-|t|/2T_1}\langle\alpha'(0)\alpha'(t)x_{10}(0)x_{10}(t)\mathrm{e}^{i\int_0^t \mathrm{d}\tau\delta\omega(\tau)}\rangle \tag{12}$$

Once again, all of the quantities contained in eq 12 are amenable to calculation within a standard MD simulation using the methods described below in Section III.

Comparing eqs 6 and 12 for the infrared and Raman line shape functions there are two significant differences. The infrared line shape function depends on the time evolution of the transition dipole of the vibration of interest ($\mu'(t)$), as opposed to the Raman line shape function, which depends on the time evolution of the transition polarizability of the vibration of interest ($\alpha'(t)$). Also, the infrared line shape function contains information regarding the rotational motion of the HOD molecule, because of its dependence on $\hat{u}(t)$, whereas the isotropic Raman line shape function is not sensitive to rotations.

III. Methods

A. Electronic Structure. The theoretical challenge to calculating infrared and isotropic Raman line shapes via eqs 6 and 12 is relating the frequency (ω), the vibrational coordinate matrix element (x_{10}), the transition dipole moment (μ'), and the isotropic

transition polarizability (α') to the instantaneous environment of the OH or OD stretch of interest. To do so we extend our ES/MD approach,[45−47,90−92] which was only concerned with ω, to the calculation of μ', α', and x_{10}.

The first step in the ES/MD approach is to extract random clusters of the solute and its local solvent environment from a short MD simulation of the solute/solvent system. These clusters are intended to form a representative sample of the environments the solute experiences in solution. We selected 100 clusters each containing a single HOD solute and between four and nine water solvent molecules from an MD simulation of the polarizable SPC-FQ model[98] of water at 298 K (more details regarding the MD simulations are discussed in Section IIIB). The simulations contained 128 water molecules, and 20 clusters were chosen from 5 independent snapshots taken at 100 ps intervals. In our previous studies of the HOD/water system we found that to recover the substantial 300 cm^{-1} (225 cm^{-1}) solvent-induced red-shift of the OH (OD) vibrational frequency of HOD, it was important to choose clusters in which the relevant hydrogen bond donor/acceptor pair (with the OH hydrogen or OD deuterium of interest as the donor) was solvated. The algorithm by which these solvated dimer clusters are taken from the simulation is detailed in ref 90.

Properly describing the vibrational properties of a water molecule in liquid water by applying ES methods to finite clusters is complicated by the ability of the water molecule to participate in extended hydrogen bond networks[113−121] and by the nonlinear cooperative effects of a water molecule simultaneously engaging in multiple hydrogen bonds.[122−124] To capture these effects we apply DFT with the B3LYP functional[125−127] and the 6-311++G** basis set to our solvated dimer clusters. All of the ES calculations were performed using the GAUSSIAN 98 software package.[128] The solvated dimer clusters are large enough to allow for extended hydrogen-bond networks, and the level of theory and basis set used in the ES calculations are sufficient to provide a reasonable description of hydrogen bonding in the cluster, including the aforementioned nonlinear cooperative effects.

The harmonic frequency of the OH or OD vibration of interest could be calculated by simply performing a normal-mode analysis on the cluster. But since each of these vibrations is to a good approximation a local mode, to obtain anharmonic frequencies instead we map the ab initio potential energy profile of the OH or OD vibration by performing eight single-point energy calculations on the cluster as the OH or OD bond of interest is stretched from 0.72 to 1.28 Å in increments of 0.08 Å. Only the H or D atom involved in the vibration is moved (in the direction of the OH or OD bond); all other atoms in the cluster are held fixed. Transition frequencies are obtained by fitting the ab initio potential curve to a Morse oscillator form,[129]

$$V(r) = D(1 - e^{-\alpha(r-r_0)})^2 \tag{13}$$

where D is the bond dissociation energy, r_0 is the equilibrium bond length, and α is a parameter that sets the range of the potential. The vibrational energy levels, E_n, for the Morse oscillator are given by

$$E_n = DB\left(n + \frac{1}{2}\right)\left[2 - B\left(n + \frac{1}{2}\right)\right] \tag{14}$$

where $n = 0, 1, 2, ...$ is the vibrational quantum number, and

$$B = \frac{\alpha\hbar}{\sqrt{2\mu D}} \tag{15}$$

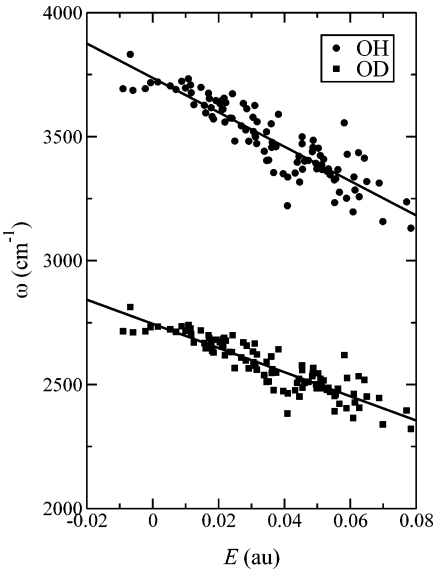

Figure 1. The symbols represent the ab initio OH or OD stretch frequency of an HOD molecule in 100 D_2O or H_2O clusters selected at random from a simulation of SPC-FQ water. These frequencies are plotted versus the electric field along the OH or OD bond due to the solvent water molecules in the cluster. The solid lines are linear fits to the data.

where μ is the reduced mass of the oscillator. An advantage to this procedure for obtaining vibrational frequencies is that they will fully reflect the effects of anharmonicity. This is essential because the degree of anharmonicity of the OH or OD stretch of HOD in water is strongly dependent on environment.

We have implicitly assumed that the vibrations of the HOD molecule are comprised of three uncoupled local modes: OH stretch, OD stretch, and HOD bend. In the gas phase this is an excellent approximation because the normal-mode eigenvectors of the isolated HOD molecule show that more than 98% of the amplitude in the OH or OD stretches is attributed to H or D motion, respectively (this is the result of a normal-mode analysis on HOD using B3LYP/6-311++G**). The local-mode approximation is even better when the molecule is in the liquid because of asymmetric solvation environments. Within the local-mode approximation the reduced mass of the OH (OD) stretch is 18/19 (34/19) amu. We have calculated the OH and OD fundamental transition frequencies ($\hbar\omega = E_1 - E_0$) of a gas-phase HOD molecule in the SPC-FQ geometry (OH and OD bond lengths of 1 Å and an HOD bond angle of 109.47°) to be 3779 and 2788 cm^{-1}, respectively. These values compare reasonably well with experiment (3707 and 2724 cm^{-1}).[130] The ratio between the measured and calculated OH and OD vibrational frequencies yields multiplicative scale factors of 0.981 and 0.977, respectively. These scale factors are used to correct all of the OH and OD vibrational frequencies in the clusters for systematic errors such as the finite basis set, incomplete incorporation of electron correlation inherent in the ab initio vibrational frequencies,[131] and errors due to the Morse fitting procedure and the local mode approximation.

In Figure 1 we show a plot of the OH and OD stretch frequencies for the 100 clusters. The OH and OD frequencies are calculated for each cluster from the same ab initio potential energy scan, but using a different reduced mass appropriate for the OH or OD oscillator (the potential obtained from the ES calculation does not depend on the isotopic masses of the nuclei in the cluster). The OH and OD frequencies are plotted versus the projection of the electric field (in atomic units) along the OH or OD bond, at the site of the H or D atom, due to the

TABLE 1: Parameters for the Linear Empirical Relationships Used in the MD Calculations of the Infrared and Isotropic Raman Spectra[a]

vibration	empirical relationship	R	rms error
OH	$\omega = 3737.0\ \text{cm}^{-1} - (6932.2\ \text{cm}^{-1}/\text{au})E$	0.90	68 cm^{-1}
OH	$x_{10} = 0.09309\ \text{Å} - (7.280 \times 10^{-6}\ \text{Å}/\text{cm}^{-1})\omega$	0.997	8.0×10^{-5} Å
OD	$\omega = 2745.8\ \text{cm}^{-1} - (4870.3\ \text{cm}^{-1}/\text{au})E$	0.90	47 cm^{-1}
OD	$x_{10} = 0.08156\ \text{Å} - (9.174 \times 10^{-6}\ \text{Å}/\text{cm}^{-1})\omega$	0.998	5.3×10^{-5} Å
both	$\mu'/\mu'_g = 1.377 + (53.03\ \text{au}^{-1})E$	0.93	0.40
both	$\alpha'/\alpha'_g = 1.271 + (5.287\ \text{au}^{-1})E$	0.56	0.15

[a] The electric field, E, along the OH or OD bond of interest is in au; frequencies, ω, are in cm^{-1}; transition dipole moments, μ', and isotropic transition polarizabilities, α', are given normalized relative to their gas-phase values, μ'_g and α'_g, respectively; and the matrix element, x_{10}, is in Å. The correlation coefficient, R, and root-mean-square error of each fit are also listed.

solvent water molecules in the cluster. The electric field variable, E, is calculated using the expression

$$E = \hat{u} \cdot \sum_{i=1}^{3n} \frac{q_i \hat{r}_{iH}}{r_{iH}^{\ 2}} \tag{16}$$

where $\hat{u}$ is a unit vector defined earlier for the OH (or OD) bond of interest, the sum is over the three charged atom-centered sites on the n SPC-FQ molecules that solvate the HOD molecule in the cluster, q_i is the charge on site i in atomic units ($e = 1$), r_{iH} is the distance between site i and the H (or D) atom of the HOD molecule in atomic units, and $\hat{r}_{iH}$ is a unit vector pointing from site i to the H (or D) atom of the HOD molecule. In the SPC-FQ model the charges on the water molecules respond to their environment, so when the clusters were extracted from the SPC-FQ simulation we also kept the current values of the charges, q_i, on all of the atomic sites for use in calculating the electric field with eq 16.

Also shown in Figure 1 are fits of the OH and OD ab initio frequencies to linear functions of E. The parameters of the fits are given in Table 1. Both of the linear fits have correlation coefficients of 0.90, with average root-mean-square deviations of 68 cm^{-1} for the OH frequencies and 47 cm^{-1} for the OD frequencies. The quality of the empirical relationship between the frequencies and E is comparable to that previously obtained for the SPC/E[97] and TIP4P[96] water models.[90,92] This relationship can be used to calculate the OH or OD frequency within an MD simulation, where E is calculated based on the charges and positions of the rest of the solvent water molecules in the simulation box (using Ewald summation to account correctly for long-range interactions and periodic boundary conditions). As in our previous work,[90−92] the range of electric fields in the clusters, and hence the range of fields over which we have confidence in our empirical fit, is more or less coincident with the range of fields in the liquid.

Buck, Buch, and co-workers have also developed a relationship between the electric field and the vibrational frequency of water by fitting the experimental infrared spectrum of $(H_2O)_7$ and $(H_2O)_8$ clusters.[71−73] Their sigmoidal form is somewhat different from the linear correlation shown in Figure 1, but would not be appropriate for use in the liquid because it was explicitly developed for gas-phase water clusters. Cho and co-workers have obtained empirical relationships between the amide I frequency of the model peptide compound NMA ($CH_3-CONH-CH_3$) in aqueous solution and the electrostatic potential on atomic sites within the NMA molecule.[67−70,75] In ref 92 we develop an empirical relationship between the amide frequency of the NMA molecule and the electric field on the central C, O, N, and H atomic sites. In the same paper we detail the differences between the electric field and electrostatic potential-based approaches for both NMA and HOD in aqueous solution.

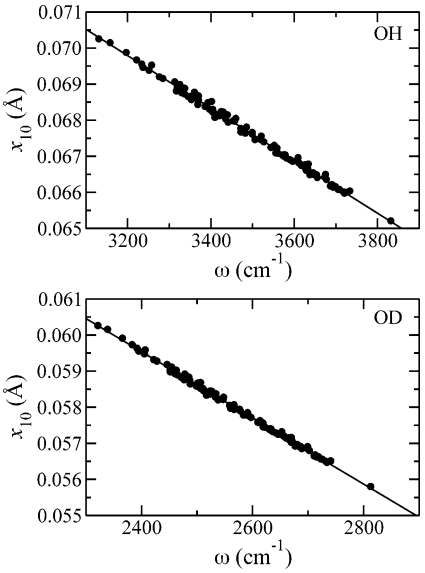

Figure 2. (a) The symbols are matrix elements of the position of the OH bond of HOD away from its equilibrium, $x = r - r_0$, between the ground and first excited vibrational states, $x_{10} = \langle 1|x|0\rangle$, for 100 HOD/$D_2O$ clusters chosen at random from a simulation of SPC-FQ water. The matrix elements are plotted as a function of the OH vibrational frequency, ω. The solid lines are linear fits of the data. (b) Same as panel a, but for the OD stretch of HOD in H_2O.

For each cluster we have fit the ab initio potential energy curve for the OH or OD vibration of interest to a Morse oscillator form whose parameters are the dissociation energy D, the range parameter α, and the equilibrium bond length r_0. In terms of these parameters, along with the reduced mass of the local mode, the matrix element of the vibrational coordinate between the ground and first excited vibrational states of the Morse oscillator is given by[132,133]

$$x_{10} = \frac{1}{\alpha(k-2)}\left[\frac{(k-1)(k-3)}{k+1}\right] \tag{17}$$

where $k = 2/B$. Using eq 17 we can calculate x_{10} for the vibrations of interest in our 100 clusters because we have access to the parameters D and α (see eq 15). However, within the MD simulation we do not calculate D and α separately for each time step; rather, we calculate the transition frequency ω from the empirical relation described above, which is implicitly a function of both D and α. So our strategy is to relate the matrix element x_{10} to the transition frequency ω. In Figure 2 we show a plot of the matrix element x_{10} versus the transition frequency ω for the OH (panel a) and OD (panel b) vibrations of our clusters. There is an excellent linear correlation between the matrix elements and the transition frequencies. The parameters of the linear fits of x_{10} to ω are listed in Table 1; the correlation coefficients of the fits are 0.997 and 0.998.

The transition dipole, μ', and isotropic transition polarizability, α', were obtained approximately for the local mode of interest within each cluster by performing a harmonic frequency calculation using the GAUSSIAN 98 electronic structure software package. GAUSSIAN reports the infrared and Raman intensities of the mode, which are each proportional to the square of the desired transition moments. The dipole moment derivatives are calculated analytically within GAUSSIAN,[134] and the isotropic Raman intensities are calculated by numerically differentiating the analytic dipole derivatives with respect to an applied electric field.

Typically, it is not meaningful to perform a harmonic frequency calculation on a cluster of molecules whose geometry is not at a local minimum of potential energy (i.e., where the forces on each atom in the cluster are zero). However, the OH stretch of an HOD molecule in a cluster of D_2O is effectively decoupled from all of the other vibrations in the cluster. This implies that the mass-weighted force constant matrix is block diagonal, and meaningful results, for the local OH stretch only, can be extracted from a harmonic frequency calculation on the cluster. We begin by optimizing the OH bond length within each of our 100 HOD·$(D_2O)_n$ clusters. The geometry optimization is accomplished by holding all atoms in the cluster fixed and allowing the position of the H atom to relax along the established OH bond direction. This step is crucial to ensure that the OH vibration is at the minimum of its potential energy. We next perform the harmonic frequency calculation within GAUSSIAN with the isotopic masses of the atoms in the cluster explicitly specified. We perform a similar calculation for the isolated HOD molecule to obtain its infrared and Raman intensities. The ratio of μ' for the clusters to that for the isolated molecule, μ'_g, is then obtained by taking the square root of the ratio of the intensities. α'/α'_g is obtained similarly. We do not need to repeat the calculations assuming HOD·$(H_2O)_n$ clusters because the transition moments, μ' and α', are intrinsically electronic properties of the water molecule and do not themselves depend on specific isotopic masses of the nuclei. Note, however, that the matrix elements x_{10} that multiply μ' and α' in eqs 6 and 12 for the infrared and isotropic Raman line shapes do depend on the reduced mass of the vibration.

In Figure 3 we show the isotropic transition polarizabilities and transition dipole moments for the OH vibration in 100 HOD·$(D_2O)_n$ clusters. α'/α'_g and μ'/μ'_g are plotted versus the projection of the electric field along the OH bond, E, given by eq 16. Qualitatively, the isotropic transition polarizabilities are not as sensitive to the local solvation environment as the transition dipole moments, which do depend sensitively on local solvation environment; indeed, they vary by over a factor of 5! These qualitative differences in dependence of α' and μ' on environment have profound consequences on the isotropic Raman and infrared line shapes discussed below in Section IV. Also shown in Figure 3 are fits of the ab initio transition moments to linear functions of E. The parameters of the fits are given in Table 1. The correlation coefficient of the linear fit of the transition dipole moments to E is 0.93 with an average root-mean-square deviation of 0.40. The correlation coefficient of the linear fit of the transition polarizabilities to E is just 0.56 with an average root-mean-square deviation of 0.15. Note that the correlation coefficient is somewhat of a misleading parameter to gauge the quality of the linear fit of α' to E because the slope of the best-fit line is very small.

B. Molecular Dynamics. MD simulations of H_2O and D_2O were performed for the SPC-FQ water model of Rick, Stuart, and Berne, details of which are described in ref 98. Our MD simulations contained 128 molecules, and the size of the cubic simulation box was chosen to give the experimental number density of H_2O or D_2O at the temperature of the simulation.[135] Periodic boundary conditions were employed, and the electrostatic forces were calculated using an approximation to the Ewald sum.[136] The classical equations of motion were integrated using the leapfrog algorithm with a 0.5 fs time step,[137] and the rotations were treated using quaternions.[138] Equilibration of the system to its desired temperature was accomplished by periodically rescaling the velocities of the molecules until the temperature was maintained to ± 1.5 K for 60 000 time steps without further adjustment. All of the results described below were computed from 1 ns constant energy trajectories. The temperature of the charge degrees of freedom[98] was maintained at 5 K by scaling the charge velocities every 1000 time steps.

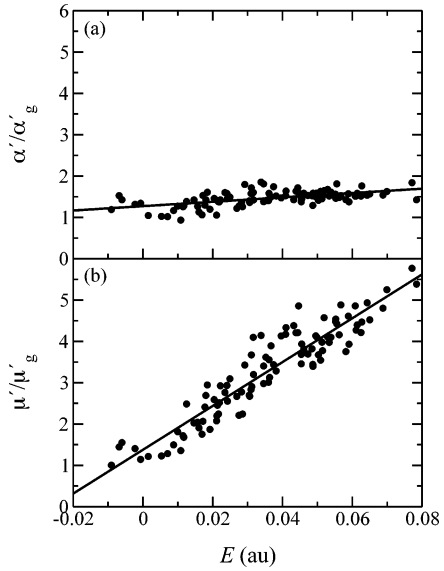

Figure 3. Shown as symbols in panel a are the scaled ab initio isotropic transition polarizabilities, α'/α'_g, for the OH (or OD) stretch of 100 HOD in D_2O (or H_2O) clusters taken from a simulation of SPC-FQ water. In panel b the symbols are scaled ab initio transition dipole moments, μ'/μ_g, for the same clusters. These quantities are plotted versus the electric field along the OH (or OD) bond due to the solvent water molecules in the cluster. The solid lines are linear fits to the data.

Our MD simulations are of the neat liquids H_2O or D_2O rather than specifically HOD in H_2O or D_2O. By simulating the neat liquid we effectively have 256 independent local modes of vibration rather than just one (i.e., we can presume that each bond in the system is the local oscillator of interest). This approximation is reasonable because the vibrational properties of the solute, HOD, are primarily modulated by the dynamics of the *solvent*. The difference in dynamics caused by replacing the HOD molecule by either an H_2O or D_2O molecule has a negligible effect on the calculated vibrational properties of the local oscillator of interest. We have previously demonstrated that the FTCF computed for the OD vibration of HOD in D_2O is numerically identical (within the noise) with that computed in a simulation of neat D_2O.[91]

IV. Results

A. Room Temperature. In Section III we used ab initio ES calculations on HOD·$(D_2O)_n$ and HOD·$(H_2O)_n$ clusters to develop empirical relationships between the projection of the electric field along the OH (or OD) bond of interest, due to the solvent, and the fundamental transition frequency (ω), transition dipole moment (μ'), and isotropic transition polarizability (α').

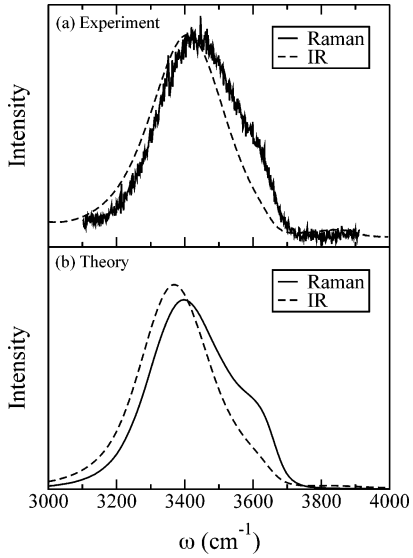

Figure 4. (a) Experimental infrared and isotropic Raman spectra of dilute HOD in D_2O at room temperature from ref 51. (b) Room-temperature IR and isotropic Raman line shapes for the OH stretch of dilute HOD in D_2O calculated for the SPC-FQ model of water.

The vibrational coordinate matrix element (x_{10}) is empirically related to the frequency. At each time step during a 1 ns MD simulation of neat D_2O (or H_2O) we calculate the electric field vector on each D (or H) due to the solvent. The electric field vector is then projected along the bond, presumed to be the OH (OD) stretch of interest if the simulation is of D_2O (H_2O). Using the projected electric field variable we can obtain trajectories of $\omega(t)$, $x_{10}(t)$, $\mu'(t)$, and $\alpha'(t)$ for each bond in the simulation. The simulations also yield $\hat{u}(t)$. These trajectories are then used in conjunction with eqs 6 and 12 to calculate the infrared and isotropic Raman line shapes for the OH or OD stretch of dilute HOD in D_2O or H_2O.

In the lower panel of Figure 4 we show our calculations for the normalized infrared and isotropic Raman line shapes for the OH stretch of HOD in D_2O at room temperature (298 K). In the upper panel are the experimental line shapes[51] for comparison (the spectra have been scaled such that their heights are approximately the same). We also note that very similar infrared and Raman line shapes were obtained by Wyss and Falk and by Walrafen.[53,59] Qualitatively, the agreement between our calculations and experiment is excellent. The infrared line shape is red-shifted relative to the Raman line shape; the Raman line shape exhibits a characteristic shoulder on the blue side (although it is a bit exaggerated in the theoretical result relative to what is seen experimentally), whereas the feature is absent in the infrared line shape; and the infrared line shape is asymmetric with a tail extending to the red. Quantitatively, the peak of the experimental infrared line shape ($\omega^* = 3407$ cm^{-1}) is red shifted 31 cm^{-1} relative to the isotropic Raman peak ($\omega^* = 3438$ cm^{-1}). In our calculations the difference in the peak locations is 28 cm^{-1}, although, in absolute terms, both calculated spectra are approximately 40 cm^{-1} too red relative to experiment (the calculated infrared line shape peaks at $\omega^* = 3369$ cm^{-1}, and the calculated Raman line shape peaks at $\omega^* = 3397$ cm^{-1}). The width (fwhm, Γ) of the calculated line shapes is also in good agreement with experiment. For the infrared calculation $\Gamma = 247$ cm^{-1}, and the experimental value is 260 cm^{-1}. For the Raman calculation $\Gamma = 310$ cm^{-1}, and the experimental value is 305 cm^{-1}.

In Figure 5 we show the results of our calculations for the normalized infrared and isotropic Raman line shapes for the

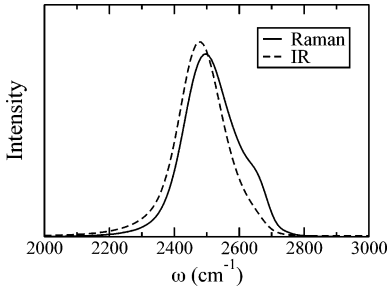

Figure 5. Room-temperature IR and isotropic Raman line shapes for the OD stretch of dilute HOD in H_2O calculated for the SPC-FQ model of water.

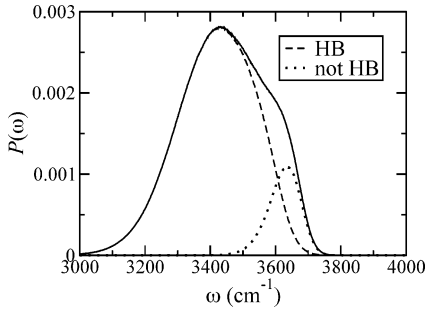

Figure 6. Room-temperature distribution of OH stretch frequencies for dilute HOD in D_2O (solid line). The distribution is shown separated into components for when the OH bond of interest is donating its proton in a hydrogen bond (HB, dashed line), and for when it is not donating a hydrogen bond (not HB, dotted line).

OD stretch of HOD in D_2O at room temperature (298 K). The agreement with experiment[46,53,56,59] (not shown) is again very good. The calculated infrared spectrum peaks at $\omega^* = 2478$ cm^{-1}, and has a width of $\Gamma = 161$ cm^{-1}. Experimentally, the analogous values are $\omega^* = 2500-2510$ cm^{-1} and $\Gamma = 162$ cm^{-1}.[46,53] The calculated isotropic Raman spectrum peaks at $\omega^* = 2498$ cm^{-1}, and has a width of $\Gamma = 185$ cm^{-1}. Experiment gives $\omega^* = 2510-2520$ cm^{-1}, and $\Gamma = 176$ cm^{-1}.[56,59]

The room-temperature isotropic Raman line shapes for the OH and OD stretch of HOD in D_2O and H_2O both exhibit shoulders on the blue side of the spectrum. This feature is also seen in the experimental line shapes, although it is slightly less pronounced, and it is absent in the infrared line shapes (both in the experiment and in our calculations). The origin of this feature in the isotropic Raman spectrum has often been attributed to the presence of two ensembles of water molecules in the liquid: those whose protons of interest are donating hydrogen bonds to neighboring water molecules, and those whose protons are not. The solid line in Figure 6 is the distribution of OH frequencies, $P(\omega)$, present in our MD simulation of D_2O; it clearly contains the characteristic shoulder. In the inhomogeneous limit, and in the limit that the transition dipole and isotropic polarizability do not depend on environment (i.e., where the Condon approximation has been employed), $P(\omega)$ is the infrared and Raman line shape. Using a geometric criterion to define if the proton of a given water molecule is participating in a hydrogen bond (i.e., the distance between the OH proton and the nearest O of another water molecule is less than 2.45 Å, and the angle between the intermolecular O- -O distance vector and the OH bond vector is less than 30°),[118,139−141] we see in Figure 6 that the distribution of frequencies can be separated into two components: one for when the proton of the OH stretch is donating a hydrogen bond (dashed curve, corresponding to 87% of the total distribution), and one when it is not (dotted curve, corresponding to 13% of the total

distribution). It is reasonable to assign the blue feature in our calculated isotropic Raman line shapes to the equilibrium subensemble of OH stretches present in the liquid that are not engaging in hydrogen bonds. This conclusion is consistent with previous findings.[40,41,51,60]

The infrared line shape lacks the blue shoulder discussed above because the transition dipole moments of the OH stretches not involved in hydrogen bonds are significantly smaller than those of the OH stretches that are involved in hydrogen bonds. In essence, the OH stretches of water molecules on the red side of the band, those that are engaging in strong hydrogen bonds, absorb more effectively than the OH stretches on the blue side of the band whose hydrogen bonds are weaker or nonexistent. Because the isotropic transition polarizabilities are virtually constant throughout the band, the Raman line shape retains the characteristic shoulder feature present in the underlying inhomogeneous distribution of frequencies. The significant sensitivity of the transition dipole moment on hydrogen bond strength, compared to the isotropic transition polarizability, also explains why the infrared spectrum is red-shifted relative to the isotropic Raman spectrum. Again, it is because there is an inherent asymmetry as to which molecules are more effective at absorbing the radiation: the red side of the infrared band is augmented, and the blue side is diminished. This results in an asymmetric spectrum that is red-shifted compared to the distribution of frequencies (and Raman spectrum).

B. Temperature-Dependent Line Shapes. MD simulations were performed to explore the effects of temperature in the range 10 to 90 °C on the infrared and isotropic Raman line shapes of HOD in H_2O and D_2O. The empirical relationships for ω, x_{10}, μ', and α' developed in Section III using water clusters from the room-temperature simulations are assumed to be applicable at other temperatures in the liquid regime. This assumption is reasonable because there are no grossly different solvation environments present at other liquid-state temperatures that are completely absent at room temperature. We also use the room-temperature values of the population relaxation time for both the OH and OD oscillators (750 fs and 1.45 ps, respectively). Actually, it is known that the OH population lifetime displays an anomalous temperature dependence; the lifetime is longer at higher temperatures.[109] At the highest temperature studied, 90 °C, the OH lifetime of HOD in D_2O is 900 fs. Incorporating this value of T_1 into the line shape calculation, as opposed to the room-temperature value, has a negligible effect on the calculated spectra (for example, the width of the infrared spectrum changes by less than 1 cm^{-1}). The temperature dependence of the lifetime of the OD oscillation of HOD in H_2O has not been measured.

Simulations of neat H_2O (for OD line shapes) and D_2O (for OH line shapes) were conducted at 10, 30, 50, 70, and 90 °C. The box size was chosen to reproduce the experimental density at each respective temperature.[142] For H_2O the densities used were 1.000, 0.996, 0.988, 0.978, and 0.965 g/cm^3. For D_2O the densities used were 1.106, 1.103, 1.096, 1.084, and 1.071 g/cm^3. The system was equilibrated to its desired temperature by periodically rescaling the velocities of the molecules until the temperature was maintained to $\pm$1.5 K for 60 000 time steps without further adjustment. The infrared and isotropic Raman line shapes were then computed from 1 ns constant energy trajectories.

In Figure 7 the infrared and isotropic Raman line shapes are shown for the OH stretch of dilute HOD in D_2O for temperatures in the range from 10 to 90 °C in increments of 20 °C. The analogous line shapes for the OD stretch of HOD in H_2O are shown in Figure 8. Qualitatively, the infrared and Raman line shapes for both OH and OD shift to the blue with increasing temperature, and decrease in overall intensity. Also, the calculated OH and OD infrared spectra are seen to broaden monotonically as temperature is increased. However, the OH and OD isotropic Raman line shapes exhibit more complex behavior than the infrared spectra, with the shoulder on the blue side of the spectrum clearly growing in relative magnitude as the temperature is increased. These same qualitative trends are observed in experimental measurements of the infrared[46,51−55] and isotropic Raman line shapes.[51,56−59]

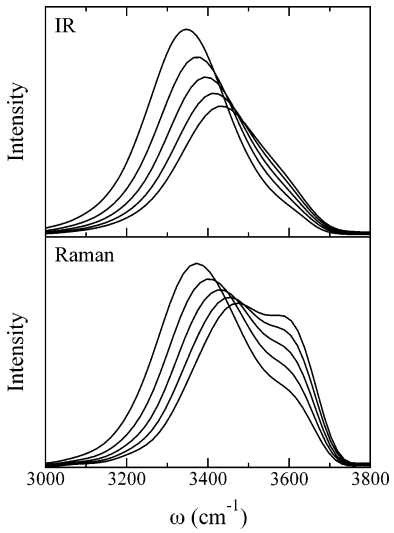

Figure 7. Calculated infrared (top panel) and isotropic Raman (lower panel) line shapes for the OH stretch of dilute HOD in D_2O at 10 (left most curve), 30, 50, 70, and 90 (right most curve) °C. As the temperature increases the spectra shift to the blue, and their peak intensity decreases.

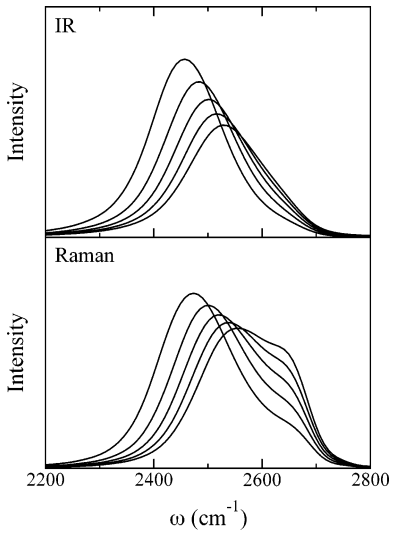

Figure 8. Calculated infrared (top panel) and isotropic Raman (lower panel) line shapes for the OD stretch of dilute HOD in H_2O at 10 (left most curve), 30, 50, 70, and 90 (right most curve) °C. As the temperature increases the spectra shift to the blue, and their peak intensity decreases.

We can also make a quantitative comparison to experiment of the trends with respect to temperature for the peak positions (ω*) and widths (Γ) of our calculated infrared and isotropic Raman spectra. In Figure 9 we compare ω* and Γ of our calculated OH and OD infrared spectra (open circles) to published experimental data from a number of different laboratories in the normal (1 atm) liquid water temperature

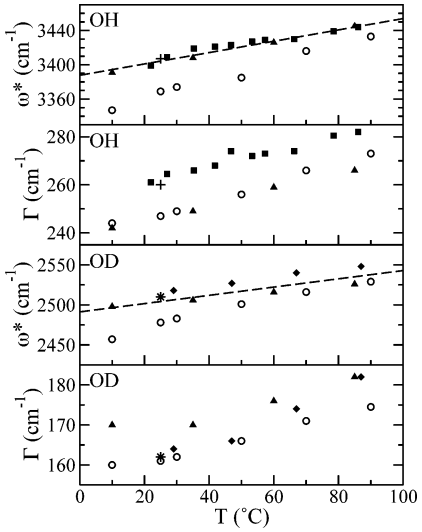

Figure 9. Calculated infrared peak positions, ω^*, and widths, Γ, for the OH and OD vibrations of dilute HOD in D_2O and H_2O plotted as a function of temperature (open circles). The other symbols and lines are experimental measurements made by various groups: (pluses) ref 51; (stars) ref 46; (filled squares) ref 52; (filled triangles) ref 53; (filled diamonds) ref 54; and (dotted line) ref 55.

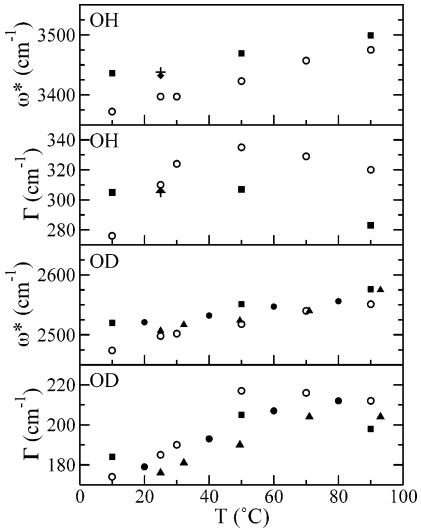

Figure 10. Calculated isotropic Raman peak positions, ω^*, and widths, Γ, for the OH and OD vibrations of dilute HOD in D_2O and H_2O plotted as a function of temperature (open circles). The other symbols and lines are experimental measurements made by various groups: (pluses) ref 51; (filled circles) ref 56; (filled squares) ref 57; (filled diamonds) ref 58; and (filled triangles) ref 59.

range.[46,51−55] In some cases the peak position and width data were explicitly reported, but in other cases only the graphed spectra were available and the parameters ω^* and Γ were extracted by magnifying the images and using a ruler to estimate them.

In the upper two panels of Figure 9 we compare the peak positions and widths of the calculated OH infrared spectra (open circles) to experiment. The experiments agree very well with one another for the peak position as a function of temperature, and the calculations reproduce the nearly linear trend of ω^* toward the blue with increasing temperature, albeit with a slightly different slope. The calculations systematically overestimate the solvent shift of the spectra by about 40 cm^{-1} at low temperature and 10 cm^{-1} at high temperature. For the widths, there is more discrepancy among the reported experimental measurements, but the trend is clear: the widths monotonically increase with increasing temperature, and this trend is again captured by our calculations. The calculated OH widths are in very good agreement with the measurements by Wyss and Falk,[53] and deviate by less than roughly 20 cm^{-1} from the measurements by Palamarev and Georgiev.[52] The most recent room-temperature measurement of the OH infrared width by Wang et al.[51] agrees more closely with Palamarev and Georgiev.

In the lower two panels of Figure 9 we compare the peak positions and widths of the calculated OD infrared spectra (open circles) to experiment. The trends are again very well reproduced by our calculations. For ω^* the experiments agree well with each other and show a monotonic shift of the peak position toward the blue with increasing temperature. As was the case for the OH infrared spectra the OD infrared spectra are systematically to the red of experiment (by about 30 cm^{-1} at low temperature and less than 10 cm^{-1} at high temperature). The calculated OD infrared line widths are in very good agreement with the measurements of Senior and Verrall,[54] which near room temperature agree well with the most recent measurement reported by Asbury et al.[46] The calculations also are within about 10 cm^{-1} of the measurements made by Wyss and Falk.[53]

In the upper two panels of Figure 10 we compare the peak positions and widths of the calculated OH isotropic Raman spectra (open circles) to experiment. As is the case for the infrared OH spectra, the experimental trend is for the isotropic Raman peak position to shift to higher frequencies as the temperature is increased. This trend is captured in our calculations, although the overall red-shift of the OH peak position relative to the gas phase is too great (by about 10 %). The width of the calculated OH isotropic Raman line shape exhibits very different behavior compared to the calculated OH infrared widths; the Raman spectrum first broadens as the temperature is increased and then narrows at higher temperature. The turnover temperature in our calculations is roughly 50 °C. This qualitative trend is also seen in the limited number of temperatures for which data are reported by Scherer et al.,[57] although there are quantitative discrepancies of roughly 30 cm^{-1} between theory and experiment. However, at room temperature the agreement between the calculated OH Raman line width and the experiments by Wang et al.[51] and by Murphy and Bernstein[58] is excellent.

In the lower two panels of Figure 10 we compare the peak positions and widths of the calculated OD isotropic Raman spectra (open circles) to experiment. The experimental trend for the OD isotropic Raman peak position to shift monotonically to the blue with increasing temperature is reproduced by the calculations. Quantitatively, the calculated peak positions agree well with experiment, although the calculations are uniformly slightly red of the experiments. The calculated OD isotropic Raman line widths first broaden with increasing temperature, until about 50 °C, at which point the line shapes narrow with increasing temperature. Three different sets of experiments also show this trend, although the turnover temperature appears to be slightly higher in the experiments.[56,57,59] The quantitative agreement between the calculated line widths and experiment is very reasonable.

Some years ago there was a lively debate about whether the Raman and infrared line shapes for dilute HOD in H_2O or D_2O displayed isosbestic points as a function of temperature.[53−55,58,59] The implications were that if they did, this provided support for the so-called "mixture" models of water, and if they did not this provided support for the "continuum" models. More recent experiments[52,56,57] seem to indicate that the isosbectic points

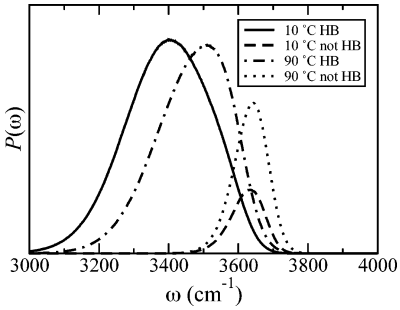

Figure 11. Shown are the distributions of OH frequencies at 10 and 90 °C of dilute HOD in D_2O separated into components for when the OH bond of interest is donating its proton in a hydrogen bond (HB), and for when it is not donating a hydrogen bond (not HB).

are only approximate. Our theoretical results in Figures 7 and 8, showing approximate isosbectic points over limited temperature ranges, are quite similar to these more recent experiments.

Given that any definition of a hydrogen bond is really quite arbitrary, there is perhaps no meaningful resolution to the old controversy regarding mixture and continuum models, and the new controversy about the number of hydrogen bonds per molecule in liquid water.[143,144] Nonetheless, to understand the temperature dependence of the line shapes, it is useful to adopt a definition of the hydrogen bond, and examine the consequences. Again choosing the usual geometric definition,[118,139−141] for the HOD/D_2O system the distribution of OH stretch frequencies can be separated into components for when the H atom is donating a hydrogen bond, and for when it is not engaged in a hydrogen bond. In Figure 11 we show the decomposition of the distribution of frequencies into hydrogen bond and non-hydrogen bond components for the lowest (10 °C) and highest (90 °C) temperatures studied. The full normalized distribution of frequencies is the sum of the two components. Two effects are apparent: the non-hydrogen bond component of the distribution of frequencies is increasing in magnitude with temperature, but its position and width remain essentially constant, and the hydrogen bond component shifts significantly to the blue (by approximately 100 cm^{-1}) and narrows (by about 50 cm^{-1}). The relative magnitude of the non-hydrogen bond component is increasing because the fraction of H atoms donating a hydrogen bond drops from 0.90 at 10 °C to 0.75 at 90 °C. The shift of the hydrogen bond component of the distribution of frequencies to the blue implies that on average hydrogen bonding in the liquid is weaker at higher temperatures. All of these effects manifest themselves in the calculated isotropic Raman spectra, as evidenced by the shoulder on the blue side of the spectra growing, and the overall blue shift and narrowing of the spectra at high temperatures. Indeed, even the nonmonotonic behavior of the Raman line widths can be understood from the frequency distributions, whose widths (for HOD/D_2O) give the nonmonotonic progression of 362, 404, 358, 340, and 316 cm^{-1} for the temperatures 10, 30, 50, 70, and 90 °C.

V. Concluding Remarks

The infrared and isotropic Raman spectra of the OH (or OD) stretch of dilute HOD in liquid D_2O (or H_2O) are qualitatively different, even though the underlying inhomogeneous distributions of frequencies and frequency fluctuation dynamics are inherently the same. The differences between these spectra are almost solely due to the dependence of the transition dipole moment on environment (i.e., the spectra would be almost identical under the Condon approximation, which assumes μ' and α' to be constant for all environments). We found that the transition dipole moment of the OH (or OD) stretch of the HOD molecule is very sensitive to its instantaneous solvent environment, as opposed to the isotropic transition polarizability, which was found to be relatively insensitive to environment. By incorporating the environmental dependence of μ' and α' into our calculations of the line shapes, we are able to recover all of the qualitative differences between the experimental infrared and Raman spectra. At room temperature the quantitative agreement between our calculated line shapes and experiment is very reasonable. In addition, we reproduce the frequency fluctuation time scales measured in some recent ultrafast vibrational echo experiments.[91] This provides support for the use of the SPC-FQ model of water in other dynamics and spectroscopy calculations.

Our calculated infrared and Raman line shapes were also able to recover the experimental trends with respect to temperature. Despite significant effects of dynamics on the spectra, the temperature dependence of the isotropic Raman line shapes mirrors that of the inhomogeneous distribution of frequencies. The shoulders present on the blue side of the isotropic Raman spectra can clearly be identified as being associated with the subensemble of non-hydrogen bonded water molecules present in the liquid, whose relative fraction increases with temperature. The underlying distribution of frequencies is obscured in the infrared spectra both because of motional narrowing, and also because the OH (or OD) oscillators that are donating a hydrogen bond have much larger transition dipole moments than those OH (or OD) stretches that are not forming hydrogen bonds with their neighbors.

An important conclusion of this work is that, at least for water, it is essential to incorporate the strong dependence of the transition dipole moment on hydrogen-bond strength and coordination in spectroscopic calculations. This was true for the infrared line shapes, which depend, effectively, on the square of the transition dipole. Certainly, it will also be important for calculations of the signal measured in ultrafast vibrational echo experiments. These signals depend on even higher powers of the transition dipole moment (μ'^4 in heterodyne experiments or μ'^8 in homodyne experiments). Incorporating the environmental dependence of the transition dipole moment in the observables measured in the ultrafast vibrational echo experiments will be the subject of a future publication.[99]

Acknowledgment. The authors would like to thank J. R. Schmidt, Chris Lawrence, and Michael Fayer for helpful discussions, Dana Dlott for providing room-temperature IR and Raman spectra of HOD in D_2O, and Andrei Tokmakoff for suggesting that we investigate how the transition dipole depends on environment from ES calculations. The authors are grateful for support from the National Science Foundation through grants CHE-0132538 and CHE-0446666. S.A.C. also acknowledges the support of a Ruth L. Kirschstein National Research Service Award administered through the National Institutes of Health.

References and Notes

(1) Mukherjee, P.; Krummel, A. T.; Fulmer, E. C.; Kass, I.; Arkin, I. T.; Zanni, M. T. *J. Chem. Phys.* **2004**, *120*, 10215.

(2) Paul, C.; Wang, J.; Wimley, W. C.; Hochstrasser, R. M.; Axelsen, P. H. *J. Am. Chem. Soc.* **2004**, *126*, 5843.

(3) Tucker, M. J.; Getahun, Z.; Nanda, V.; DeGrado, W. F.; Gai, F. *J. Am. Chem. Soc.* **2004**, *126*, 5078.

(4) Getahun, Z.; Huang, C.-Y.; Wang, T.; León, B. D.; DeGrado, W. F.; Gai, F. *J. Am. Chem. Soc.* **2003**, *125*, 405.

(5) Huang, C.-Y.; Wang, T.; Gai, F. *Chem. Phys. Lett.* **2003**, *371*, 731.

(6) Suydam, I. T.; Boxer, S. G. *Biochemistry* **2003**, *42*, 12050.

(7) Reimers, J. R.; Hall, L. E. *J. Am. Chem. Soc.* **1999**, *121*, 3730.
(8) Fulmer, E. C.; Mukherjee, P.; Krummel, A. T.; Zanni, M. T. *J. Chem. Phys.* **2004**, *120*, 8067.
(9) Bredenbeck, J.; Hamm, P. *J. Chem. Phys.* **2003**, *119*, 1569.
(10) Khalil, M.; Demirdöven, N.; Tokmakoff, A. *J. Chem. Phys. A* **2003**, *107*, 5258.
(11) Woutersen, S.; Pfister, R.; Hamm, P.; Mu, Y.; Kosov, D. S.; Stock, G. *J. Chem. Phys.* **2002**, *117*, 6833.
(12) Woutersen, S.; Hamm, P. *J. Chem. Phys.* **2001**, *115*, 7737.
(13) Woutersen, S.; Hamm, P. *J. Chem. Phys.* **2001**, *114*, 2727.
(14) Zanni, M. T.; Asplund, M. C.; Hochstrasser, R. M. *J. Chem. Phys.* **2001**, *114*, 4579.
(15) Zanni, M. T.; Gnanakaran, S.; Stenger, J.; Hochstrasser, R. M. *J. Phys. Chem. B* **2001**, *105*, 6520.
(16) Asplund, M. C.; Zanni, M. T.; Hochstrasser, R. M. *Proc. Natl. Acad. Sci. U.S.A.* **2000**, *97*, 8219.
(17) Woutersen, S.; Hamm, P. *J. Phys. Chem. B* **2000**, *104*, 11316.
(18) Hamm, P.; Lim, M.; DeGrado, W. F.; Hochstrasser, R. M. *Proc. Natl. Acad. Sci. U.S.A.* **1999**, *96*, 2036.
(19) Hamm, P.; Lim, M.; DeGrado, W. F.; Hochstrasser, R. M. *J. Phys. Chem. A* **1999**, *103*, 10049.
(20) Scheurer, C.; Piryatinski, A.; Mukamel, S. *J. Am. Chem. Soc.* **2001**, *123*, 3114.
(21) Dreyer, J.; Moran, A. M.; Mukamel, S. *J. Phys. Chem. B* **2003**, *107*, 5967.
(22) Moran, A.; Mukamel, S. *Proc. Natl. Acad. Sci. U.S.A.* **2004**, *101*, 506.
(23) Lee, C.; Cho, M. *J. Phys. Chem. B* **2004**, *108*, 20397.
(24) Wang, Z.; Pang, Y.; Dlott, D. *J. Chem. Phys.* **2004**, *120*, 8345.
(25) Loparo, J. J.; Fecko, C. J.; Eaves, J. D.; Roberts, S. T.; Tokmakoff, A. *Phys. Rev. B* **2004**, *70*, 180201.
(26) Fecko, C. J.; Loparo, J. J.; Roberts, S. T.; Tokmakoff, A. *J. Chem. Phys.* **2005**, *122*, 054506.
(27) Nibbering, E. T. J.; Elsaesser, T. *Chem. Rev.* **2004**, *104*, 1887.
(28) Fecko, C. J.; Eaves, J. D.; Loparo, J. J.; Tokmakoff, A.; Geissler, P. L. *Science* **2003**, *301*, 1698.
(29) Yeremenko, S.; Pshenichnikov, M. S.; Wiersma, D. A. *Chem. Phys. Lett.* **2003**, *369*, 107.
(30) Pakoulev, A.; Wang, Z.; Dlott, D. D. *Chem. Phys. Lett.* **2003**, *371*, 594.
(31) Pakoulev, A.; Wang, Z.; Pang, Y.; Dlott, D. D. *Chem. Phys. Lett.* **2003**, *380*, 404.
(32) Stenger, J.; Madsen, D.; Hamm, P.; Nibbering, E. T. J.; Elsaesser, T. *J. Phys. Chem. A* **2002**, *106*, 2341.
(33) Stenger, J.; Madsen, D.; Hamm, P.; Nibbering, E. T. J.; Elsaesser, T. *Phys. Rev. Lett.* **2001**, *87*, 027401.
(34) Gallot, G.; Lascoux, N.; Gale, G. M.; Leicknam, J.-C.; Bratos, S.; Pommeret, S. *Chem. Phys. Lett.* **2001**, *341*, 535.
(35) Bakker, H. J.; Woutersen, S.; Nienhuys, H.-K. *Chem. Phys.* **2000**, *258*, 233.
(36) Bratos, S.; Gale, G. M.; Gallot, G.; Hache, F.; Lascoux, N.; Leicknam, J.-C. *Phys. Rev. E* **2000**, *61*, 5211.
(37) Deàk, J. C.; Rhea, S. T.; Iwaki, L. K.; Dlott, D. D. *J. Phys. Chem. A* **2000**, *104*, 4866.
(38) Gale, G. M.; Gallot, G.; Hache, F.; Lascoux, N.; Bratos, S.; Leicknam, J.-C. *Phys. Rev. Lett.* **1999**, *82*, 1068.
(39) Woutersen, S.; Bakker, H. J. *Phys. Rev. Lett.* **1999**, *83*, 2077.
(40) Laenen, R.; Rauscher, C.; Laubereau, A. *Phys. Rev. Lett.* **1998**, *80*, 2622.
(41) Laenen, R.; Rauscher, C.; Laubereau, A. *J. Phys. Chem. B* **1998**, *102*, 9304.
(42) Woutersen, S.; Emmerichs, U.; Bakker, H. J. *Science* **1997**, *278*, 658.
(43) Graener, H.; Seifert, G.; Laubereau, A. *Phys. Rev. Lett.* **1991**, *66*, 2092.
(44) Steinel, T.; Asbury, J. B.; Zheng, J.; Fayer, M. D. *J. Phys. Chem. A* **2004**, *108*, 10958.
(45) Steinel, T.; Asbury, J. B.; Corcelli, S. A.; Lawrence, C. P.; Skinner, J. L.; Fayer, M. D. *Chem. Phys. Lett.* **2004**, *386*, 295.
(46) Asbury, J. B.; Steinel, T.; Stromberg, C.; Corcelli, S. A.; Lawrence, C. P.; Skinner, J. L.; Fayer, M. D. *J. Phys. Chem. A* **2004**, *108*, 1107.
(47) Asbury, J. B.; Steinel, T.; Kwak, K.; Corcelli, S. A.; Lawrence, C. P.; Skinner, J. L.; Fayer, M. D. *J. Chem. Phys.* **2004**, *121*, 12431.
(48) Laenen, R.; Simeonidis, K.; Laubereau, A. *J. Phys. Chem. B* **2002**, *106*, 408.
(49) Lock, A. J.; Bakker, H. J. *J. Chem. Phys.* **2002**, *117*, 1708.
(50) Kropman, M. F.; Nienhuys, H.-K.; Woutersen, S.; Bakker, H. J. *J. Phys. Chem. A* **2001**, *105*, 4622.
(51) Wang, Z.; Pakoulev, A.; Pang, Y.; Dlott, D. *J. Phys. Chem. A* **2004**, *108*, 9054.
(52) Palamarev, H.; Georgiev, G. *Vib. Spectrosc.* **1994**, *7*, 255.
(53) Wyss, H. R.; Falk, M. *Can. J. Chem.* **1970**, *48*, 607.
(54) Senior, W. A.; Verrall, R. E. *J. Phys. Chem.* **1969**, *73*, 4242.
(55) Falk, M.; Ford, T. A. *Can. J. Chem.* **1966**, *44*, 1699.
(56) Hare, D. E.; Sorensen, C. M. *J. Chem. Phys.* **1990**, *93*, 6954.
(57) Scherer, J. R.; Go, M. K.; Kint, S. *J. Phys. Chem.* **1974**, *78*, 1304.
(58) Murphy, W. F.; Bernstein, H. J. *J. Phys. Chem.* **1972**, *76*, 1147.
(59) Walrafen, G. E. *J. Chem. Phys.* **1968**, *48*, 244.
(60) Wang, Z.; Pakoulev, A.; Pang, Y.; Dlott, D. *Chem. Phys. Lett.* **2003**, *378*, 281.
(61) Møller, K. B.; Rey, R.; Hynes, J. T. *J. Phys. Chem. A* **2004**, *108*, 1275.
(62) Lawrence, C. P.; Skinner, J. L. *Chem. Phys. Lett.* **2003**, *369*, 472.
(63) Lawrence, C. P.; Skinner, J. L. *J. Chem. Phys.* **2003**, *118*, 264.
(64) Rey, R.; Møller, K. B.; Hynes, J. T. *J. Phys. Chem. A* **2002**, *106*, 11993.
(65) Lawrence, C. P.; Skinner, J. L. *J. Chem. Phys.* **2002**, *117*, 5827.
(66) Lawrence, C. P.; Skinner, J. L. *J. Chem. Phys.* **2002**, *117*, 8847.
(67) Ham, S.; Kim, J.-H.; Lee, H.; Cho, M. *J. Chem. Phys.* **2003**, *118*, 3491.
(68) Kwac, K.; Cho, M. *J. Chem. Phys.* **2003**, *119*, 2247.
(69) Kwac, K.; Cho, M. *J. Chem. Phys.* **2003**, *119*, 2256.
(70) Choi, J.; Ham, S.; Cho, M. *J. Phys. Chem. B* **2003**, *107*, 9132.
(71) Sadlej, J.; Buch, V.; Kazimirski, J. K.; Buck, U. *J. Phys. Chem. A* **1999**, *103*, 4933.
(72) Brudermann, J.; Melzer, M.; Buck, U.; Kazimirski, J. K.; Sadlej, J.; Buch, V. *J. Chem. Phys.* **1999**, *110*, 10649.
(73) Buck, U.; Ettischer, I.; Melzer, M.; Buch, V.; Sadlej, J. *Phys. Rev. Lett.* **1998**, *80*, 2578.
(74) Diraison, M.; Guissani, Y.; Leicknam, J.-C.; Bratos, S. *Chem. Phys. Lett.* **1996**, *258*, 348.
(75) Cho, M. *J. Chem. Phys.* **2003**, *118*, 3480.
(76) Reimers, J. R.; Watts, R. O. *Chem. Phys.* **1984**, *91*, 201.
(77) Ojamäe, L.; Hermansson, K.; Probst, M. *Chem. Phys. Lett.* **1992**, *191*, 500.
(78) Ojamäe, L.; Tegenfeldt, J.; Lindgren, J.; Hermansson, K. *Chem. Phys. Lett.* **1992**, *195*, 97.
(79) Bour, P.; Keiderling, T. *J. Chem. Phys.* **2003**, *119*, 11253.
(80) Hayashi, T.; la Cour Jansen, T.; Zhuang, W.; Mukamel, S. *J. Phys. Chem. A* **2005**, *109*, 64.
(81) Huggins, C. M.; Pimentel, G. C. *J. Phys. Chem.* **1956**, *60*, 1615.
(82) Pimentel, G. C.; McClellan, A. L. *The Hydrogen Bond*; W. H. Freeman and Company: San Francisco, CA, 1960.
(83) Glew, D. N.; Rath, N. S. *Can. J. Chem.* **1971**, *49*, 837.
(84) Whalley, E.; Klug, D. D. *J. Chem. Phys.* **1986**, *84*, 78.
(85) Hermansson, K.; Knuts, S.; Lindgren, J. *J. Chem. Phys.* **1991**, *95*, 7486.
(86) Matsuoka, O.; Clementi, E.; Yoshimine, M. *J. Chem. Phys.* **1976**, *64*, 1351.
(87) Wojcik, M. J.; Hermansson, K.; Lindgren, J.; Ojamäe, L. *Chem. Phys.* **1993**, *171*, 189.
(88) Morita, A.; Hynes, J. T. *J. Phys. Chem. B* **2002**, *106*, 673.
(89) Morita, A.; Hynes, J. T. *Chem. Phys.* **2000**, *258*, 371.
(90) Corcelli, S. A.; Lawrence, C. P.; Skinner, J. L. *J. Chem. Phys.* **2004**, *120*, 8107.
(91) Corcelli, S. A.; Lawrence, C. P.; Asbury, J. B.; Steinel, T.; Fayer, M. D.; Skinner, J. L. *J. Chem. Phys.* **2004**, *121*, 8897.
(92) Schmidt, J. R.; Corcelli, S. A.; Skinner, J. L. *J. Chem. Phys.* **2004**, *121*, 8897.
(93) Hermansson, K. *J. Chem. Phys.* **1993**, *99*, 861.
(94) Hayashi, T.; Hamaguchi, H.-O. *Chem. Phys. Lett.* **2000**, *326*, 115.
(95) Williams, R. B.; Loring, R. F.; Fayer, M. D. *J. Phys. Chem. B* **2001**, *105*, 4068.
(96) Jorgensen, W. L.; Chandrasekhar, J.; Madura, J. D.; Impey, R. W.; Klein, M. L. *J. Chem. Phys.* **1983**, *79*, 926.
(97) Berendsen, H. J. C.; Grigera, J. R.; Straatsma, T. P. *J. Phys. Chem.* **1987**, *91*, 6269.
(98) Rick, S. W.; Stuart, S. J.; Berne, B. J. *J. Chem. Phys.* **1994**, *101*, 6141.
(99) Schmidt, J. R.; Corcelli, S. A.; Skinner, J. L. *J. Chem. Phys.*, in press.
(100) Xu, H.; Stern, H. A.; Berne, B. J. *J. Phys. Chem. B* **2002**, *106*, 2054.
(101) Head-Gordon, T.; Hura, G. *Chem. Rev.* **2002**, *102*, 2651.
(102) Soper, A. K. *Chem. Phys.* **2000**, *258*, 121.
(103) Stephens, M. D.; Saven, J. G.; Skinner, J. L. *J. Chem. Phys.* **1997**, *106*, 2129.
(104) Mukamel, S. *Principles of Nonlinear Optical Spectroscopy*; Oxford University Press: New York, 1995.
(105) Saven, J. G.; Skinner, J. L. *J. Chem. Phys.* **1993**, *99*, 4391.
(106) Fried, L. E.; Mukamel, S. *Adv. Chem. Phys.* **1993**, *84*, 435−516.
(107) Oxtoby, D. W.; Levesque, D.; Weis, J.-J. *J. Chem. Phys.* **1978**, *68*, 5528.
(108) Gale, G. M.; Gallot, G.; Lascoux, N. *Chem. Phys. Lett.* **1999**, *311*, 123.

(109) Woutersen, S.; Emmerichs, U.; Nienhuys, H.-K.; Bakker, H. J. *Phys. Rev. Lett.* **1998**, *81*, 1106.
(110) Everitt, K. F.; Skinner, J. L. *J. Chem. Phys.* **2001**, *115*, 8531.
(111) Levesque, D.; Weis, J.-J.; Oxtoby, D. W. *J. Chem. Phys.* **1980**, *72*, 2744.
(112) McQuarrie, D. A. *Statistical Mechanics*; Harper and Row: New York, 1976.
(113) Modig, K.; Pfommer, B. G.; Halle, B. *Phys. Rev. Lett.* **2003**, *90*, 075502.
(114) Sutmann, G.; Vallauri, R. *J. Mol. Liq.* **2002**, *98*−*9*, 215.
(115) Bergman, D. L. *Chem. Phys.* **2000**, *253*, 267.
(116) Ohmine, I.; Saito, S. *Acc. Chem. Res.* **1999**, *32*, 741.
(117) Mishima, O.; Stanley, H. E. *Nature* **1998**, *396*, 329.
(118) Luzar, A.; Chandler, D. *Phys. Rev. Lett.* **1996**, *76*, 928.
(119) Matsumoto, M.; Ohmine, I. *J. Chem. Phys.* **1996**, *104*, 2705.
(120) Shiratani, E.; Sasai, M. *J. Chem. Phys.* **1996**, *104*, 7671.
(121) Stillinger, F. H. *Science* **1980**, *209*, 451.
(122) Weinhold, F. *J. Mol. Struct.* (*THEOCHEM*) **1997**, *398*−*399*, 181.
(123) Keutsch, F. N.; Saykally, R. J. *Proc. Natl. Acad. Sci. U.S.A.* **2001**, *98*, 10533.
(124) Cruzan, J. D.; Braly, L. B.; Liu, K.; Brown, M. G.; Loeser, J. G.; Saykally, R. J. *Science* **1996**, *271*, 59.
(125) Becke, A. D. *J. Chem. Phys.* **1993**, *98*, 5648.
(126) Lee, C.; Yang, W.; Parr, R. G. *Phys. Rev. B* **1988**, *37*, 785.
(127) Miehlich, B.; Savin, A.; Stoll, H.; Preuss, H. *Chem. Phys. Lett.* **1989**, *157*, 200.
(128) Frisch, M. J.; Trucks, G. W.; Schlegel, H. B.; Scuseria, G. E.; Robb, M. A.; Cheeseman, J. R.; Zakrzewski, V. G.; Montgomery, J. A., Jr.; Stratmann, R. E.; Burant, J. C.; Dapprich, S.; Millam, J. M.; Daniels, A. D.; Kudin, K. N.; Strain, M. C.; Farkas, O.; Tomasi, J.; Barone, V.; Cossi, M.; Cammi, R.; Mennucci, B.; Pomelli, C.; Adamo, C.; Clifford, S.; Ochterski, J.; Petersson, G. A.; Ayala, P. Y.; Cui, Q.; Morokuma, K.; Malick, D. K.; Rabuck, A. D.; Raghavachari, K.; Foresman, J. B.; Cioslowski, J.; Ortiz, J. V.; Baboul, A. G.; Stefanov, B. B.; Liu, G.; Liashenko, A.; Piskorz, P.; Komaromi, I.; Gomperts, R.; Martin, R. L.; Fox, D. J.; Keith, T.; Al-Laham, M. A.; Peng, C. Y.; Nanayakkara, A.; Challacombe, M.; Gill, P. M. W.; Johnson, B.; Chen, W.; Wong, M. W.; Andres, J. L.; Gonzalez, C.; Head-Gordon, M.; Replogle, E. S.; Pople, J. A. *Gaussian 98*; Gaussian Inc.: Pittsburgh, PA, 1998.
(129) Corcelli, S. A.; Kelley, J. A.; Tully, J. C.; Johnson, M. A. *J. Phys. Chem. A* **2002**, *106*, 4872.
(130) Benedict, W. S.; Gailar, N.; Plyler, E. K. *J. Chem. Phys.* **1956**, *24*, 1139.
(131) Scott, A. P.; Radom, L. *J. Phys. Chem.* **1996**, *100*, 16502.
(132) Vasan, V. S.; Cross, R. J. *J. Chem. Phys.* **1983**, *78*, 3869.
(133) Gallas, J. A. C. *Phys. Rev. A* **1980**, *21*, 1829.
(134) Yamaguchi, Y.; Frisch, M.; Gaw, J.; Schaefer, H. F.; Binkley, J. S. *J. Chem. Phys.* **1986**, *84*, 2262.
(135) Franks, F., Ed. *Water: A Comprehensive Treatise*; Plenum Press: New York, 1972; Vol. 1.
(136) Adams, D. J.; Dubey, G. S. *J. Comput. Phys.* **1987**, *72*, 156.
(137) Allen, M. P.; Tildesley, D. J. *Computer Simulation of Liquids*; Clarendon: Oxford, UK, 1987.
(138) Svanberg, M. *Mol. Phys.* **1997**, *92*, 1085.
(139) Luzar, A. *J. Chem. Phys.* **2000**, *113*, 10663.
(140) Luzar, A.; Chandler, D. *Nature* **1996**, *379*, 55.
(141) Luzar, A.; Chandler, D. *J. Chem. Phys.* **1993**, *98*, 8160.
(142) Eisenberg, D.; Kauzmann, W. *The Structure and Properties of Water*; Oxford University Press: New York, 1969.
(143) Wernet, P.; Nordlund, D.; Bergmann, U.; Cavalleri, M.; Odelius, M.; Ogasawara, H.; Naslund, L. A.; Hirsch, T. K.; Ojamae, L.; Glatzel, P.; Pettersson, L. G. M.; Nilsson, A. *Science* **2004**, *304*, 995.
(144) Smith, J. D.; Cappa, C. D.; Wilson, K. R.; Messer, B. M.; Cohen, R. C.; Saykally, R. J. *Science* **2004**, *306*, 851.